Journal of Sound and Vibration (2002) **257**(2), 337–359
doi:10.1006/jsvi.5043, available online at http://www.idealibrary.com on IDEAL®

NON-LINEAR BEAM OSCILLATIONS EXCITED BY LATERAL FORCE AT COMBINATION RESONANCE

K. V. Avramov

Department of Theoretical Mechanics, National Technical University "Kharkov Polytechnical Institute", Frunze St. 21, *Kharkov* 61002, *Ukraine. E-mail*: *avramov@kvavr.kharkov.ua*

(*Received* 1 *June* 2001, *and in final form* 28 *November* 2001)

Non-linear oscillations of a beam subjected to a periodic force at a combination resonance are considered. Using the Galerkin method, a partial differential equation of oscillations is reduced to a system of ordinary differential equations with a small parameter. A system of three autonomous differential equations is derived, the multiple scales method being used. Qualitative properties of trajectories are analyzed. The Naimark–Sacker bifurcations at the combination resonance are analyzed by the center manifold method. Almost-periodic oscillations of a beam arise due to these bifurcations. These oscillations are investigated qualitatively and numerically.

1. INTRODUCTION

Many engineering structures can be modelled as beam-like continuous systems. For finite motions, the linear equations show poor approximation of the system's response. Therefore, the study of the non-linear dynamics of beams is an important problem. Many efforts have been made to analyze this problem. Researchers considered the oscillations in a plane or in a non-plane. Various problems of free plane oscillations caused interests for researchers. The influence of midplane stretching on free vibrations was analyzed by Woinowsky-Krieger [1] and by Langley [2]. Wagner [3] considered coupled longitudinal and transverse free oscillations of beam. In this paper the non-linear relation for curvature was used. Many-mode approximation of free oscillations is considered by McDonald and Raleigh [4]. Evensen [5] applied the perturbation techniques to solve the partial differential equation of free oscillations. A beam with geometric and physical properties that vary along the length was considered by Nayfeh [6]. He took into account the transverse shear and the rotary inertia.

Many papers considered beam oscillations subjected to longitudinal and lateral forces. A one-mode approximation of oscillations subjected to lateral forces was studied by many researches. Tseng and Dugundj [7, 8] analyzed beam oscillations excited by base motions. Note that vibrations were considered as the product of a generalized coordinate and the first buckling mode. Taking into account a longitudinal inertia, Luongo, *et al.* [9] obtained an ordinary differential equation of beam vibrations. Lou and Sikarskie [10] considered oscillations as the product of a generalized coordinate and the spatial variable function. We stress that this function was not the flexural mode. Beam oscillations subjected to the longitudinal and lateral periodic forces were considered by Fung [11]. He took into account longitudinal inertia. Dong *et al.* [12] pointed to one application of non-linear beam theory. They analyzed the vortex-induced oscillations of leg platform tethers.

0022-460X/02/$35.00

Many-mode approximations of beams oscillations have been considered by many scientists. Bennet and Eisley [13, 14] analyzed two-mode approximations of beam oscillations. Series were used to analyze vibrations in reference [15]. The obtained equations were solved by the multiple scales method. Tang and Dowell [16] studied a beam subjected to a periodic force. This beam was arranged between two magnets. A book [17] contains the non-linear theory for beams.

The attention of scientists was drawn to plane oscillations of beams subjected to periodic longitudinal forces. Taking into account the longitudinal inertia, column dynamics was studied by Evensen and Evan-Iwanowsky [18]. Rotary inertia and beam longitudinal oscillations were considered by Eisinger and Merchant [19]. Parametric oscillations of a beam with the disk were analyzed by Sato *et al.* [20]. Oscillations of a viscoelasticity beam were studied by Kovalov and Rozovski [21]. Hoang-Van-Da [22] studied beam oscillations taking into account the stress–deformation nonlinear ratio. Parametric oscillations theory is considered in a book [23].

Non-planar oscillations of a beam appear due to the unstability of plane motions. Crespo da Silva [24, 25] considered free non-planar oscillations. He took into account a longitudinal inertia. Luongo *et al.* [26] analyzed beam motions when the bending and torsional natural frequencies were commensurable. Unstable plane motions were investigated by Haight and King [27]. In the case of these motions, non-planar oscillations are stable. Forced non-planar oscillations were studied in references [28–30].

Planar oscillations of a beam subjected to a lateral force are considered in the present paper. It is known that combination resonances are dangerous [17]. Therefore, the investigations of non-linear beam oscillations under the conditions of combination resonances are an actual problem, which is considered in this paper. Many-mode approximation of oscillations is used. The Naimark–Sacker bifurcations leading to almost-periodic oscillations are discovered. We stress that these motions have significant amplitudes. The center manifold method is used to study the above-mentioned bifurcations.

2. THE PROBLEM FORMULATION

A beam with fixed ends experiences a midplane stretching when deflected. The influence of this stretching on the response increases with the motion amplitude. This situation can be described by non-linear strain–displacement equations and a linear stress–strain law which give the nonlinear beam equation. Consider a hinged–hinged beam as shown in Figure 1. For such a beam the partial differential equation of plane motion has the form [15, 31]:

$$\begin{gathered}\rho A W_{tt} + \beta W_t + EJ W_{xxxx} = \frac{EA}{2l} W_{xx} \int_0^l W_x^2 \, \mathrm{d}x + F(x,t), \\ W|_{x=0} = W|_{x=l} = W_{xx}|_{x=0} = W_{xx}|_{x=l} = 0,\end{gathered} \tag{1}$$

where $F(x,t) = F_0 \delta(x - l/3)\cos(\Omega_1 t)$ is the periodic force; $\delta(\ )$ is the delta function; W is the beam deflection; $(EA/2l)\int_0^l W_x^2 \mathrm{d}x$ is the tension due to midplane stretching; ρ is the beam material density; E is Young's modulus; A, J are an area and second moment of area of a cross-section. Now introduce the dimensionless parameters and variables:

$$\sqrt{\varepsilon} W^* = \frac{W}{r}, \quad x^* = \frac{x}{l}, t^* = \sqrt{\frac{EJ}{\rho A l^4}} t, \frac{\beta l^2}{Ar\sqrt{E\rho}} = 2\mu\varepsilon,$$

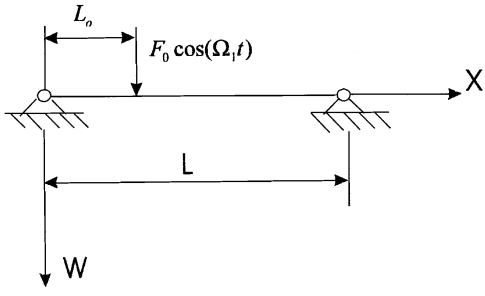

Figure 1. The physical system.

$$\sqrt{\varepsilon} f_0 = \frac{l^3 F_0}{EJr}, \quad \delta\left(x^* - \frac{1}{3}\right) = l\delta\left(x - \frac{l}{3}\right), \tag{2}$$

where $\varepsilon \ll 1; r$ is a cross-section of radius gyration. Now present equation (1) with respect to the dimensionless variables and parameters herewith dropping the asterisk in the notation:

$$W_{tt} + W_{xxxx} = \varepsilon\left(\frac{1}{2} W_{xx} \int_0^1 W_x^2 \, \mathrm{d}x - 2\mu W_t\right) + f(x,t), \tag{3}$$

where $f(x,t) = f_0\delta(x - \frac{1}{3})\cos(\Omega t)$. A many-mode approximation

$$W = \sqrt{2}\sum_n \eta_n(t)\sin(n\pi x)$$

is used to analyze the oscillations. Using the Galerkin method, the ordinary differential equations are obtained

$$\ddot{\eta}_k + \omega_k^2 \eta_k = \varepsilon\left(-\frac{\pi^4}{2} k^2 \eta_k \sum_{i=1}^{\infty} i^2 \eta_i^2 - 2\mu\dot{\eta}_k\right) + 2h_k \cos(\Omega t),$$

$$\omega_k = k^2\pi^2, \quad h_k = \frac{f_0}{\sqrt{2}} \sin\left(\frac{k\pi}{3}\right), \quad k = 1, 2, \ldots . \tag{4}$$

Combination resonance requires the relation $2\Omega = 5\pi^2 + \varepsilon\sigma$. Some other resonances (primary, subharmonic and superharmonic) are analyzed in reference [17]. The multiple scales method [32, 33] is applied to solve equations (4). The change of the variables:

$$\eta_k = a_k \cos(k^2\pi^2 t + \beta_k) + 2\Lambda_k \cos(\Omega t) + O(\varepsilon),$$
$$\Lambda_k = \frac{4h_k}{\pi^4(4k^4 - 25)} \tag{5}$$

is used to obtain the modulation equations:

$$
\begin{gathered}
a_1' + \mu a_1 + 4Fa_2 \sin(\sigma T_1 - \beta_1 - \beta_2) = 0,\\
-a_1\beta_1' + \frac{3}{16}\pi^2 a_1^3 + H_1 a_1 + \frac{\pi^2}{2} a_1\left(a_2^2 + \frac{9}{4}a_3^2\right) + 4Fa_2\cos(\sigma T_1 - \beta_1 - \beta_2) = 0,\\
a_2' + \mu a_2 + Fa_1 \sin(\sigma T_1 - \beta_1 - \beta_2) + \frac{9\pi^2}{2}\Lambda_2\Lambda_3 a_3 \sin(\beta_3 - \beta_2 - \sigma T_1) = 0,\\
-a_2\beta_2' + \frac{3}{4}\pi^2 a_2^3 + H_2 a_2 + \frac{\pi^2}{8} a_2(a_1^2 + 9a_3^2) + Fa_1\cos(\sigma T_1 - \beta_1 - \beta_2)\\
+\frac{9\pi^2}{2}\Lambda_2\Lambda_3 a_3\cos(\beta_3 - \beta_2 - \sigma T_1) = 0,\\
a_3' + \mu a_3 - 2\pi^2\Lambda_2\Lambda_3 a_2 \sin(\beta_3 - \beta_2 - \sigma T_1) = 0,\\
-a_3\beta_3' + \frac{27}{16}\pi^2 a_3^3 + H_3 a_3 + \pi^2\frac{a_3}{8}\left(a_1^2 + 4a_2^2\right) + 2\pi^2\Lambda_2\Lambda_3 a_2\cos(\beta_3 - \beta_2 - \sigma T_1) = 0,\\
a_k' + \mu a_k = 0; k = 4, 5, ...,
\end{gathered}
\tag{6}
$$

where $T_1 = \varepsilon t, (\ )' = \dfrac{\mathrm{d}(\ )}{\mathrm{d}T_1}, F = (\pi^2/2)\Lambda_1\Lambda_2;$

$$
\begin{aligned}
H_1 &= \frac{3}{2}\pi^2\Lambda_1^2 + \frac{\pi^2}{2}\sum_{v=2}^{\infty} v^2\Lambda_v^2,\\
H_2 &= 6\pi^2\Lambda_2^2 + \frac{\pi^2}{2}\sum_{v\neq 2} v^2\Lambda_v^2,\\
H_3 &= \frac{27}{2}\pi^2\Lambda_3^2 + \frac{\pi^2}{2}\sum_{v\neq 3} v^2\Lambda_v^2.
\end{aligned}
\tag{7}
$$

From equations (6), we derive that $a_k = 0, k = 4, 5, \ldots, .$ Using equations (4), (6) and (7), system (6) is transformed into the following equations:

$$
\begin{gathered}
\gamma' - \sigma + \frac{5}{16}\pi^2 a_1^2 + \frac{5}{4}\pi^2 a_2^2 + \frac{6f_0^2\chi}{\pi^6} - \frac{f_0^2\chi_1}{\pi^6}\left(\frac{4a_2}{a_1} + \frac{a_1}{a_2}\right)\cos(\gamma) = 0,\\
a_1' + \mu a_1 - 4\frac{f_0^2}{\pi^6}\chi_1 a_2 \sin(\gamma) = 0,\\
a_2' + \mu a_2 - \frac{f_0^2}{\pi^6}\chi_1 a_1 \sin(\gamma) = 0,
\end{gathered}
\tag{8}
$$

where $\gamma = \sigma T_1 - \beta_1 - \beta_2; \chi_1 = 3{\cdot}7 \times 10^{-3};$

$$
\chi = \frac{3285}{670761} + \sum_{m=0}^{\infty}\frac{(3m+1)^2}{(4(3m+1)^4 - 25)^2} + \sum_{m=0}^{\infty}\frac{(3m+2)^2}{(4(3m+2)^4 - 25)^2} = 9{\cdot}82 \times 10^{-3}. \tag{9}
$$

Series (9) are convergent and their sums were calculated approximately. Equations (8) have the form:

$$
\begin{aligned}
x' &= -\mu x - \left(\sigma - \frac{6f_0^2\chi}{\pi^6}\right)y + \frac{5}{16}\pi^2(z^2 + 4x^2 + 4y^2)y - 4\frac{f_0^2\chi_1}{\pi^6}\frac{xy}{z},\\
y' &= \left(\sigma - \frac{6f_0^2\chi}{\pi^6}\right)x - \mu y + \frac{f_0^2\chi_1}{\pi^6}z - \frac{5}{16}\pi^2(z^2 + 4x^2 + 4y^2)x + 4\frac{f_0^2\chi_1}{\pi^6}\frac{x^2}{z},\\
z' &= -\mu z + 4\frac{f_0^2\chi_1}{\pi^6}y,
\end{aligned}
\tag{10}
$$

where $(x, y, z) = (a_2 \cos\gamma; a_2 \sin\gamma; a_1)$. Note that the non-autonomous differential equations (4) are transformed into a the system of three autonomous equations.

Limit cycles, homoclinic orbits and chaos are observed in three-dimensional dynamical systems [34–37]. We stress that these trajectories were discovered in the modulation equations of different mechanical systems [38–40]. Therefore, it is natural to assume, that these phenomena may take place in system (10).

Note that the divergence of the vector field (10) has the form:

$$\frac{\partial x'}{\partial x} + \frac{\partial y'}{\partial y} + \frac{\partial z'}{\partial z} = -3\mu - 4\frac{f_0^2\chi_1}{\pi^6}\frac{y}{z}. \tag{11}$$

It is stressed that it depends on the state variables. If orbits come up on the plane $z = 0$, the values of the divergence tend to $\pm\infty$.

Using equations (5) and (6), beam oscillations are derived in the form

$$W = \sqrt{2}a_1 \cos(\pi^2 t + \beta_1)\sin(\pi x) + \sqrt{2}a_2 \cos(4\pi^2 t + \beta_2)\sin(2\pi x) + \psi(x, t) + O(\varepsilon),$$

$$\psi(x,t) = \frac{4\sqrt{3}f_0}{\pi^4}\left\{\sum_{m=0}^{\infty}\frac{(-1)^m \sin[(3m+1)\pi x]}{4(3m+1)^4 - 25} + \sum_{m=0}^{\infty}\frac{(-1)^m \sin[(3m+2)\pi x]}{4(3m+2)^4 - 25}\right\}\cos(\Omega t). \tag{12}$$

Note that the steady and transient beam oscillations correspond to the same solutions of system (10).

3. PHASE SPACE QUALITATIVE PROPERTIES

Let us study the flow $\phi_t(x, y, z)$ of system (10). Note that equations (8) and (10) are invariant with respect to transformations

$$(a_1, a_2) \to (-a_1, -a_2); \qquad (x, y, z) \to (-x, -y, -z). \tag{13}$$

System (10) is symmetrical. The theory of symmetrical dynamical systems is expounded in reference [41]. Let us prove the theorem.

Theorem 1. *If x or y is not infinitesimal, flow $\phi_t(x, y, z)$ does not intersect the plane $z = 0$.*

Proof. Let us consider the orbits from the first octant $(z > 0, x > 0, y > 0)$. Using equation (10), the following limits are obtained:

$$\lim_{z\to 0} z' = 4\frac{f_0^2\chi_1}{\pi^6}y, \qquad \lim_{z\to 0} y' = \infty, \quad \lim_{z\to 0} x' = -\infty. \tag{14, 15}$$

It follows from equation (14), that such values of t exist that the orbits approaching the plane $z = 0$ begin to move away from it. Therefore, these trajectories do not intersect the plane $z = 0$. Now consider the motions meeting the relations: $x < 0; y > 0; z > 0$. Then equation (14) and limits are true:

$$\lim_{z\to 0} x' = \infty, \quad \lim_{z\to 0} y' = \infty. \tag{16}$$

As inequality $z' > 0$ is true, the conclusion for the first octant is correct. Let us analyze the trajectories when $x > 0; y > 0; z < 0$. Then formula (14) and limits are true:

$$\lim_{z\to -0} x' = \infty; \quad \lim_{z\to -0} y' = -\infty. \tag{17}$$

As inequality $z > 0$ is met, the trajectories approach the plane $z = 0$. However, the variable y becomes negative due to equation (17) and the fulfilment of inequality $z' < 0$ follows

from (14). Therefore, such values of t exist that the trajectories start to move away from plane $z = 0$. Lastly consider the trajectories from the sixth octant: $y > 0; x < 0; z < 0$. Then, formula (14) and limits are fulfilled:

$$\lim_{z \to -0} x' = -\infty, \quad \lim_{z \to -0} y' = -\infty. \tag{18}$$

Meeting equations (14) and (18), the trajectories approach the plane $z = 0$ while $y > 0$. However, variable y becomes negative and the trajectories move away from the plane $z = 0$. It follows from equation (13) that motions occur in just the same way in the others octants. QED.

Note that system (10) has a fixed point $x = y = z = 0$. Let us prove the theorem on this point.

Theorem 2. *Only one asymptotically stable fixed point* $x = y = z = 0$ *is observed in dynamical system* (10) *at* $f_0 < \pi^3 \sqrt{\mu}/\sqrt{2\chi_1}$. *There are no other steady states.*

Proof. Consider the Liapunov function:

$$V = x^2 + y^2 + \frac{(r + \sqrt{r^2 - 4})^2}{16} z^2, \tag{19}$$

where $r = \pi^6 \mu / f_0^2 \chi_1$. The function $\dot{V}$ has the form:

$$\frac{\dot{V}}{\mu} = -2x^2 - 2\left(y - \frac{r + \sqrt{r^2 - 4}}{4} z\right)^2 < 0. \tag{20}$$

It follows from the theorem on global stability [42] that fixed the point $x = y = z = 0$ is globally asymptotically stable at $r^2 > 4$. The theorem inequality follows from the last relation.

Thus, if $f_0 < \pi^3 \sqrt{\mu}/\sqrt{2\chi_1}$, only one steady motion of a beam is observed. This motion meets formula (12) at $a_1 = a_2 = 0$.

Definition. Trajectories are called "approaching the origin" and "moving away from the origin", if the following inequalities are met:

$$(x, y, z) \cdot (\dot{x}, \dot{y}, \dot{z}) = x\dot{x} + y\dot{y} + z\dot{z} < 0 \tag{21}$$

and

$$(x, y, z) \cdot (\dot{x}, \dot{y}, \dot{z}) > 0 \tag{22}$$

respectively. Let us choose the sphere $(x^2 + y^2 + z^2 = R^2)$ in the phase space to explain this definition. If trajectories enter this sphere, they approach the origin. Now let us prove the following theorem.

Theorem 3. *If inequality* $5f_0^2 \chi_1 / 2\pi^6 > \mu$ *is met, the trajectories move away from the origin in the domain*

$$K_+ = \left\{ (x, y, z) \in R^3 \setminus -\mu x^2 - \mu y^2 - \mu z^2 + 5\frac{f_0^2 \chi_1}{\pi^6} yz > 0 \right\} \tag{23}$$

and the trajectories approach the origin in the domain

$$K_- = \left\{ (x, y, z) \in R^3 \setminus -\mu x^2 - \mu y^2 - \mu z^2 + 5\frac{f_0^2 \chi_1}{\pi^6} yz < 0 \right\}. \tag{24}$$

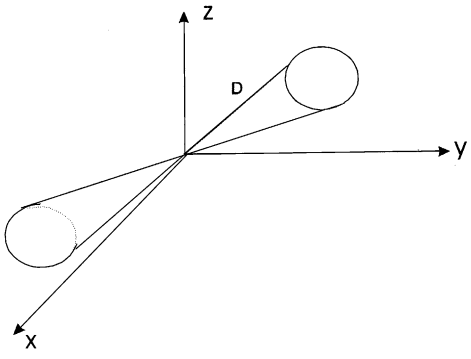

Figure 2. The boundary of two regions.

Proof. System (10) meets the relation

$$(x, y, z) \cdot (\dot{x}, \dot{y}, \dot{z}) = -\mu x^2 - \mu y^2 - \mu z^2 + 5\frac{f_0^2 \chi_1}{\pi^6} yz. \tag{25}$$

Inequalities (23) and (24) are obtained from equation (25) and inequalities (21,22).

Let us denote the boundary between domains K_+ and K_- by D:

$$D = \left\{ (x, y, z) \in R^3 \setminus -\mu x^2 - \mu y^2 - \mu z^2 + 5\frac{f_0^2 \chi_1}{\pi^6} yz = 0 \right\}. \tag{26}$$

Figure 2 shows this boundary. Note that D does not depend on σ.

Theorem 4. *If a limit cycle, a chaotic attractor or a homoclinic orbit are observed in dynamical system* (10), *then such orbits pass through domains K_+ and K_-.*

Proof. Let us give the proof for limit cycles, as the proofs are similar for the others kinds of trajectories. The cycle does not approach the origin and does not move away from it if it lies on the sphere $x^2 + y^2 + z^2 = R^2$. As system (10) meets the relation: $(d/dt)(x^2 + y^2 + z^2) \neq 0$, the cycles do not lie on a sphere. This means that limit cycles approach the origin and move away from it. Thus we conclude that these cycles pass through domains K_+ and K_-.

4. DYNAMICAL SYSTEM FIXED POINTS

4.1. ANALYSIS OF LINEAR APPROXIMATION

System (8) has a fixed point $(a_1, a_2) = (0, 0)$. Other fixed points of this system satisfy the equations:

$$\begin{gathered} a_1 = 2a_2, \\ 4\mu^2 + \left(\frac{6f_0^2 \chi}{\pi^6} - \sigma + \frac{5}{8}\pi^2 a_1^2 \right)^2 = 16\frac{f_0^4 \chi_1^2}{\pi^{12}}. \end{gathered} \tag{27}$$

The solutions of these equations are

$$a_1^{(A,B)} = \frac{2\sqrt{2}}{\sqrt{5}\pi} \sqrt{\sigma - \frac{6f_0^2 \chi}{\pi^6} \pm p}, \tag{28}$$

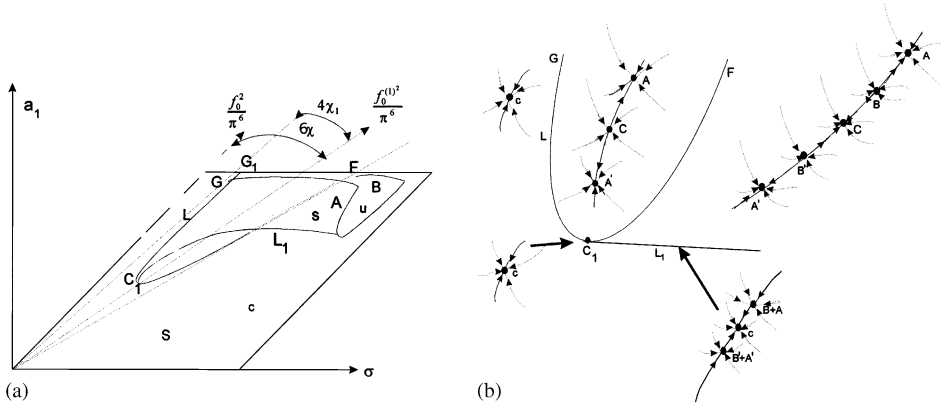

Figure 3. (a) The amplitude surface of beam oscillations; (b) the bifurcation diagram.

where $p^2 = 16f_0^4\chi_1^2/\pi^{12} - 4\mu^2$. Let us denote two fixed points of equation (28) by $r_A = (x_A, y_A, z_A)$, $r_B = (x_B, y_B, z_B)$. The following formulae are derived:

$$x_{A,B} = \pm\frac{\pi^5 p}{2\sqrt{10}f_0^2\chi_1}\sqrt{\sigma - \frac{6f_0^2\chi}{\pi^6} \pm p}, \quad y_{A,B} = \frac{\pi^5\mu}{\sqrt{10}f_0^2\chi_1}\sqrt{\sigma - \frac{6f_0^2\chi}{\pi^6} \pm p},$$
$$z_{A,B} = \frac{4}{\sqrt{10}\pi}\sqrt{\sigma - \frac{6f_0^2\chi}{\pi^6} \pm p}. \tag{29}$$

Theorem 5. *Fixed points r_A and r_B lie on surface D.*

Proof. If formulae (29) are substituted into equation (26), the latest is true.

A response surface is a suitable geometric characteristic to present fixed points. A response surface was used to analyze the Duffing oscillator in reference [43]. Let us use this surface to analyze the fixed points of system (8). In this case, the response surface (Figure 3) shows the fixed points– $\sigma - f_0^2/\pi^6$ relation. Note that the section of this surface is a frequency response. The surface consists of sheets A, B, C. Sheet C corresponds to the fixed point $a_1 = a_2 = 0$. Sheets A and B show the fixed points denoted by the same letters. The sheets of the stable and unstable fixed points are denoted by S and U respectively. We stress that if the system parameters meet the inequality

$$f_0 > \pi^3\sqrt{\frac{\mu}{2\chi_1}}, \tag{30}$$

the significant amplitudes appear. Note that if Theorem 2 condition is violated, fixed points r_A and r_B appear.

Let us calculate the eigenvalues and eigenvectors of the Jacobi matrix to study the fixed points stability and to determine the linearized invariant manifolds [42]. The eigenvalues and eigenvectors of the fixed points r_A and $r_B - \lambda_i^{(A)}$, $V_i^{(A)}$ and $\lambda_i^{(B)}$, $V_i^{(B)}$

have the form:

$$\lambda_1^{(A,B)} = -2\mu, \quad \lambda_{2,3}^{(A)} = -\mu \pm R_1, \quad \lambda_{2,3}^{(B)} = -\mu \pm R_2,$$
$$V_1^{(A,B)} = \begin{pmatrix} \mp\frac{p}{2} \\ -\mu \\ \frac{4f_0^2\chi_1}{\pi^6} \end{pmatrix}, \quad V_2^{(A,B)} = \begin{pmatrix} \pm\frac{p}{2} \pm \frac{2\mu}{p}(\mu - R_{1,2}) \\ R_{1,2} \\ \frac{4f_0^2\chi_1}{\pi^6} \end{pmatrix}, \tag{31}$$
$$V_3^{(A,B)} = \begin{pmatrix} \pm\frac{p}{2} \pm \frac{2\mu}{p}(\mu + R_{1,2}) \\ -R_{1,2} \\ \frac{4f_0^2\chi_1}{\pi^6} \end{pmatrix},$$

where $R_{1,2} = \sqrt{\mu^2 \mp \frac{5}{8}\pi^2 a_1^2 p}$. If the fixed point r_A has complex conjugate eigenvalues $\lambda_{2,3}^{(A)}$, the eigenvectors $V_{2,3}^{(A)}$ are

$$V_2^{(A)} = \begin{pmatrix} \frac{p}{2} \\ -\mu \\ \frac{4f_0^2\chi_1}{\pi^6} \end{pmatrix}, \quad V_3^{(A)} = \begin{pmatrix} -\frac{\mu}{r}\left(\frac{p}{2} + \frac{5}{4}\pi^2 a_1^2\right) \\ r \\ \frac{-4\mu f_0^2\chi_1}{\pi^6 r} \end{pmatrix}, \tag{32}$$

where $r = \sqrt{\frac{5}{8}\pi^2 a_1^2 p - \mu^2}$. The linearized invariant manifolds have the form [44]:

$$E^s = span[V_1^{(A)}, V_2^{(A)}, V_3^{(A)}], \quad E^s = span[V_1^{(B)}, V_3^{(B)}], \quad E^u = span[V_2^{(B)}], \tag{33}$$

where E^s, E^u are the stable and unstable subspaces of the linearized system. As follows from formulae (29) and (31), the following inequalities are met:

$$r_B \cdot V_i^{(B)} > 0, \quad i = 1, 3. \tag{34}$$

As follows from equation (34), the manifolds $W(r_B)$ of the fixed point r_B meet Theorem 3. If R_1 is real, the eigenvectors of the fixed point r_A satisfy the inequality: $r_A \cdot V_i^{(A)} > 0$. For complex conjugate $\lambda_{2,3}^{(A)}$, the linearized invariant manifold is the plane $span[V_2^{(A)}, V_3^{(A)}]$. Figure 4 shows this manifold. Note that the trajectories of this manifold meet Theorem 3.

Let us consider the fixed point $a_1 = a_2 = 0$. Eigenvalues λ_i of this point are

$$\lambda_1 = -2\mu, \quad \lambda_{2,3} = -\mu \pm \sqrt{4\frac{f_0^4\chi_1^2}{\pi^{12}} - \frac{1}{4}\left(\sigma - \frac{6f_0^2\chi}{\pi^6}\right)^2}. \tag{35}$$

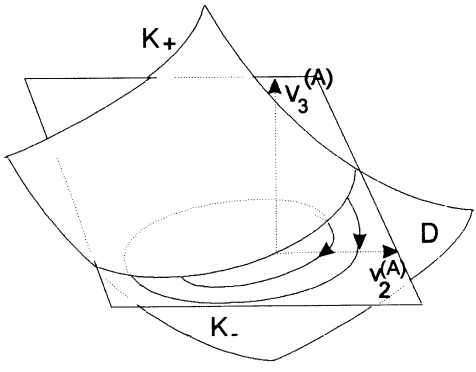

Figure 4. The linearized invariant manifolds of fixed point A.

If $\lambda_{2,3}$ are real, the vectors U_1, U_2, U_3 have the form:

$$U_1 = \begin{pmatrix} 1 \\ 0 \\ 0 \end{pmatrix}, \quad U_2 = \begin{pmatrix} -\frac{1}{2}\left(\sigma - \frac{6f_0^2\chi}{\pi^6}\right) \\ \sqrt{4\left(\frac{f_0^2\chi_1}{\pi^6}\right)^2 - \frac{1}{4}\left(\sigma - \frac{6f_0^2\chi}{\pi^6}\right)^2} \\ \frac{4f_0^2\chi_1}{\pi^6} \end{pmatrix}, \quad U_3 = \begin{pmatrix} -\frac{1}{2}\left(\sigma - \frac{6f_0^2\chi}{\pi^6}\right) \\ -\sqrt{4\left(\frac{f_0^2\chi_1}{\pi^6}\right)^2 - \frac{1}{4}\left(\sigma - \frac{6f_0^2\chi}{\pi^6}\right)^2} \\ \frac{4f_0^2\chi_1}{\pi^6} \end{pmatrix}. \tag{36}$$

If $\lambda_{2,3}$ are complex conjugate, U_2 and U_3 are

$$U_2 = \left(0; -\sqrt{\frac{1}{4}\left(\sigma - \frac{6f_0^2\chi}{\pi^6}\right)^2 - 4\left(\frac{f_0^2\chi_1}{\pi^6}\right)^2}; 0\right)^{\mathrm{T}}, \quad U_3 = \left(-\frac{1}{2}\left(\sigma - \frac{6f_0^2\chi}{\pi^6}\right); 0; \frac{4f_0^2\chi_1}{\pi^6}\right)^{\mathrm{T}}. \tag{37}$$

The linearized invariant manifolds have the form:

$$\begin{aligned} &\lambda_2 < 0, \quad E^s = span[U_1, U_2, U_3], \\ &\lambda_2 = 0, \quad E^c = span[U_2], \quad E^s = span[U_1; U_3], \\ &\lambda_2 > 0, \quad E^u = span[U_2], \quad E^s = span[U_1; U_3], \end{aligned} \tag{38}$$

where E^c is the central subspace of the linearized system. Note that the Poincare–Andronov–Hopf bifurcation does not appear in system (10).

The non-hyperbolic fixed points of sheet C meet equation $\lambda_2 = 0$. This equation has the form

$$\left(\sigma - \frac{6f_0^2\chi}{\pi^6}\right)^2 = 16\frac{f_0^4\chi_1^2}{\pi^{12}} - 4\mu^2. \tag{39}$$

Let us introduce coordinate axis $(\sigma^{(1)},\ f_0^{(1)^2}/\pi^6)$ obtained by the rotation of axis $\left(\sigma, \frac{f_0^2}{\pi^6}\right)$ on angle $\alpha = -6\chi$ (Figure 3(a)). Then equation (39) takes the form

$$-\frac{\sigma^{(1)^2}}{4\mu^2} + \left(\frac{f_0^{(1)^2}}{\pi^6}\right)^2 \frac{4\chi_1^2}{\mu^2} = 1. \tag{40}$$

This formula is the equation of the hyperbola, which separates the stable fixed points from the unstable fixed points. Curves (GC_1) and (C_1F) show the supercritical and subcritical symmetric pitchfork bifurcations respectively. Co-dimension two bifurcation point C_1 separates the supercritical bifurcation curve from the subcritical bifurcation curve.

As follows from equation (35), eigenvalues $\lambda_{2,3}$ are real in the region bounded by lines $(G_1O), (FO)$ and curve L (Figure 3(a)). The eigenvalues are complex outside this region.

Theorem 6. *If eigenvalues $\lambda_{2,3}$ of fixed point $a_1 = a_2 = 0$ are real, the following statements are correct.*

(1) Linearized invariant manifold U_2 is stable, if it is situated in domain K_- and this manifold is unstable, if it is situated in K_+.
(2) Nonhyperbolic fixed point $a_1 = a_2 = 0$ has $U_2 \in D$.
(3) Linearized invariant manifolds U_1, U_3 are situated in K_-.

Proof. The region of unstable fixed point $a_1 = a_2 = 0$ (see Figure 3(a)) meets the inequality:

$$\left(\sigma - \frac{6f_0^2\chi}{\pi^6}\right)^2 < 16\frac{f_0^4\chi_1^2}{\pi^{12}} - 4\mu^2. \tag{41}$$

If the components of vector U_2 (see equation (36)) are substituted into inequality (24), relation (41) is obtained. The first statement is proved. If the components of vector U_2 are substituted into equation (26), formula (39) is obtained. This proves the second statement. If the components of vectors U_1, U_3 are substituted into equation (24), the inequalities meeting at any values of σ, f_0, μ are obtained. The third statement is proved too.

Let us consider the orbits close to the stable fixed point $a_1 = a_2 = 0$ with complex $\lambda_{2,3}$. In this case, it is easily shown that the condition $span[U_2, U_3] \in K_-$ is met. Therefore, the trajectories on linearized manifold $span[U_2, U_3]$ meet Theorem 3.

The response surface contains saddle-node bifurcation curve L_1. Sheets A and B are joined along this curve. Eigenvalues $\lambda_i; i = \overline{1,3}$ of the curve L fixed points are $\lambda_1 = \lambda_2 = -2\mu; \lambda_3 = 0$. We stress that at $f_0 = \pi^3\sqrt{\mu/2\chi_1}$, the frequency response contains co-dimension two bifurcation point C_1 and bifurcation curve L_1.

4.2. CENTER MANIFOLDS APPLICATION FOR THE BIFURCATIONS ANALYSIS

Center manifolds method [42, 44] is used to analyze the dynamics close to co-dimension two bifurcation point C_1. This method reduces a system dimension. Note that local bifurcations take place on center manifolds. Changing parameter $\delta = \sigma - 6f_0^2\chi/\pi^6$, system (10) bifurcations are considered. To analyze the trajectories close to point $x = y = z = 0$

we derive equations (10) in the new form:

$$\begin{pmatrix} x' \\ y' \\ z' \end{pmatrix} = \begin{pmatrix} -2\mu & 0 & 0 \\ 0 & -\mu & v\chi_1 + \dfrac{\mu}{2} \\ 0 & 4\chi_1 v + 2\mu & -\mu \end{pmatrix} \begin{pmatrix} x \\ y \\ z \end{pmatrix} + \begin{pmatrix} -\dfrac{\delta}{4}\left(2y + \dfrac{\mu}{2\chi_1 v + \mu}\right) z + \dfrac{5\pi^2}{16}(z^2 + 4x^2 + 4y^2)y \\ -\dfrac{\delta^2 z}{8(2\chi_1 v + \mu)} - \dfrac{5\pi^2}{16}(z^2 + 4x^2 + 4y^2)x \\ 0, \end{pmatrix}, \tag{42}$$

where $v = f_0^2/\pi^6 - \mu/2\chi_1$. Bifurcation point C_1 is observed at $v = \delta = 0$. Therefore parameters v and δ are assumed small. System (42) is derived in eigenbasis $(u, v, w) = (x; y + z/2; z/2 - y)$:

$$\begin{aligned} u' &= -2\mu u + r_1(u, v, w, \delta), \\ v' &= 2\chi_1 v v + r_2(u, v, w, \delta), \\ w' &= -2(\mu + \chi_1 v)w - r_2(u, v, w, \delta). \end{aligned} \tag{43}$$

Appendix A contains functions $r_1(u, v, w, \delta)$ and $r_2(u, v, w, \delta)$. The center manifold has the form of the power series:

$$\begin{aligned} u &= -\frac{v\delta}{4(2\chi_1 v + \mu)} + \frac{5\pi^2 v^3}{32(3\chi_1 v + \mu)} + O(4), \\ w &= \frac{v\delta^2}{16(\mu + 2\chi_1 v)^2} + O(4), \end{aligned} \tag{44}$$

where symbol $O(4)$ denotes the terms of order $v^4; \delta v^3; \delta^2 v^2; \delta^3 v; \delta^4$. The restriction of vector field (10) on the center manifold is

$$v' = a_1 v + a_2 v^3 + a_3 v^5 + O(v^7), \tag{45}$$

where

$$a_1 = 2\chi_1 v - \frac{\delta^2}{8\mu} + O(\delta^4), \quad a_2 = \frac{5\pi^2\delta}{32\mu}\left[1 + \frac{\delta^2}{8\mu^2} + O(\delta^4)\right], \quad a_3 = -\frac{25\pi^4}{256\mu}\left[1 + \frac{3\delta^2}{8\mu^2} + O(\delta^4)\right].$$

Note that equation (45) meets the symmetrical property $v \to -v$, which is the Ruelle theorem consequence [41]. System (45) describes the bifurcations close to point C_1. If $16\mu\chi_1 v > \delta^2$, fixed point $v = 0$ is unstable. This point describes sheet C. System (45) bifurcation curve meets equation $16\mu\chi_1 v = \delta^2$. This equation approximates curve L close to C_1. Equation (45) on curve L has the following form:

$$v' = \frac{5\pi^2\delta}{32\mu} v^3 + O(v^5). \tag{46}$$

Note that at $\delta < 0$ the manifold is stable and it is unstable at $\delta > 0$. The fixed points of equation (45) have the form

$$v^*_{1,2} = \frac{8}{5\pi^2}\sqrt{\delta \pm 4\sqrt{\chi_1 v \mu}}. \tag{47}$$

Fixed points v_1^* and v_2^* describe sheets A and B respectively. Equation (45) on point C_1 is derived in the form

$$v' = -\frac{25\pi^4}{256\mu}v^5 + O(v^7). \tag{48}$$

Therefore, point C_1 is stable.

Let us consider the saddle-node bifurcation L_1 (Figure 3(a)) close to bifurcation point C_1. We introduce the new variables

$$x_1 = x, \quad y_1 = y - 2\sqrt{\delta_1}, \quad z_1 = z - 4\sqrt{\delta_1}, \tag{49}$$

where $10\pi^2\delta_1 = \delta$. Then system (10) has the form:

$$\begin{pmatrix} x_1' \\ y_1' \\ z_1' \end{pmatrix} = \begin{pmatrix} -2\mu & \delta & \frac{\delta}{2} \\ 0 & -\mu & \frac{\mu}{2} \\ 0 & 2\mu & -\mu \end{pmatrix} \begin{pmatrix} x_1 \\ y_1 \\ z_1 \end{pmatrix} + \begin{pmatrix} f_1 \\ f_2 \\ f_3 \end{pmatrix}. \tag{50}$$

Appendix A contains the functions f_1, f_2, f_3. System (50) is written in the eigenbasis $(u, v, w) = (x_1 - (\delta/2\mu)y_1 - (\delta/4\mu)z_1, (\delta/4\mu)(2y_1 + z_1), z_1/2 - y_1)$:

$$u' = -2\mu u + F_1, \qquad v' = F_2, w' = -2\mu w + F_3. \tag{51}$$

Appendix A contains functions F_1, F_2, F_3. The center manifold is $u = a_1v^2 + b_1vv + c_1v^2 + O(3); w = a_2v^2 + b_2vv + c_2v^2 + O(3)$, where $O(3)$ denotes the terms of order $v^3; v^2v; vv^2; v^3$. Parameters $a_1, b_1, c_1, a_2, b_2, c_2$ are defined according to the center manifold method [42]. The vector field (10) restriction on the center manifold has the form

$$v' = -v^3\left(\frac{5\pi^2\mu}{2\delta} + \frac{5\delta\pi^2}{8\mu}\right) - \frac{\pi\sqrt{10\delta}}{4}v^2 + 2\chi_1 vv + \frac{4\chi_1 v\delta^{\frac{3}{2}}}{\sqrt{10}\mu\pi} + O(v^4). \tag{52}$$

Equation (52) describes the saddle-node bifurcation in system (10). Fixed points $v_{1,2} = \mp(2/\pi)\sqrt{2\chi_1\delta v/5\mu} + O(v)$ define two branches of bifurcation diagram. The stability of these points is defined by $\lambda_{1,2} = \pm 2\delta\sqrt{\chi_1 v/\mu} + O(v)$. The saddle-node bifurcation curve is $v = 0$. The trajectories close to point C_1 are shown on bifurcation diagram (Figure 3(b)). Fixed points C and B correspond to the sheets with the same notations (Figure 3(a)). Note that the phase space contains the heteroclinic orbits. Heteroclinic orbits $(BA), (BC), (B'C), (B'A')$ are structurally stable in region (FC_1L_1) (see Figure 3b). Two structurally stable heteroclinic orbits (CA) and (CA') take place in region (GLC_1F).

Note that similar dynamics is discovered in two-degree-of-freedom mechanical system [45].

Recall that all fixed points lie on the surface D. Let us analyze the heteroclinic orbits close to C_1 from this point of view. As follows from Theorem 6, if the system parameters are found in the region (GLC_1F) (Figure 3(b)), heteroclinic orbits (CA) and (CA') lie in K_+. If the system parameters are found in the region (FC_1L_1), heteroclinic orbits (BC) and $(B'C)$ lie in K_-.

5. MODULATION EQUATION NUMERICAL ANALYSIS

Calculations were carried out in two stages. At the first stage we sought steady states different from the fixed points. Let us take the parameter $\mu = 0{\cdot}05$. We fix the parameters σ and f_0 to explain the approach. Let us fill uniformly phase space domain $A_1' = [(x, y, z) \in R^3 \setminus -5 < x < 5; -5 < y < 5; 1 \times 10^{-4} < z < 5]$ with the points. The number of these points was equal to 64. Every point was taken as initial conditions to solve

numerically system (10). If the motion reached a steady state (the fixed point, a limit cycle or a chaotic attractor), the integration was stopped and the next initial conditions were chosen and the integration was repeated. Such calculations were developed for all points. Afterwards the value of σ or f_0 was changed and the calculations were repeated. The region $A_2'' = [(\sigma, f_0) \in R^2 \setminus -100 \leqslant \sigma \leqslant 100; 400 \leqslant f_0 \leqslant 9000]$ was filled with 280 points and every point was analyzed. As the result of the calculations we come to the conclusion that in the whole region A_2'' all motions are attracted to the stable fixed points.

Invariant manifolds of the fixed points were analyzed at the second stage of the calculations. The algorithm from reference [46] was used. Equation (10) has the singularity at $z = 0$. Therefore, this algorithm was changed a little in the following way. If the linearized invariant manifold of fixed point $x = y = z = 0$ belongs to plane (xoy), equations (42) are solved at the first step of the numerical integration. Afterwards equations (10) are solved. The calculations were developed at the different values of μ, σ, f_0. These parameters were changed according to the following procedure. We fixed the parameter μ. The domain of σ and f_0 variation was $A' = [(\sigma, f_0) \in R^2 \setminus \sigma_{min} < \sigma < \sigma_{max},\ f_0^{min} < f_0 < f_0^{max}]$. We set this variation in the form: $\sigma_i = \sigma_{min} + ih_\sigma^{(i)},\ f_{0,k} = f_0^{min} + kh_f^{(k)},\ 1 \leqslant i \leqslant i_{max}; 1 \leqslant k \leqslant k_{max}$. Thus region A' was filled with points. The number of these points was $N_p = i_{max}k_{max}$. The invariant manifolds were calculated for every point. The amount of the calculations is presented in Table 1. The values of μ are presented in the first column. Domain A' and the values of N_p are indicated in the second and third columns, respectively. Figure 5 shows the invariant manifolds of the fixed point $a_1 =$

TABLE 1

The calculation description

μ	A'	N_p
2	$0 < \sigma < 180; 512{\cdot}8 < f_0 < 1400$	54
0·6	$0 < \sigma < 1500; 290 < f_0 < 4270$	105
0·05	$0 < \sigma < 1500; 100 < f_0 < 4600$	45
0·001	$0 < \sigma < 1500; 70 < f_0 < 3800$	51
0·0001	$0 < \sigma < 1500; 15 < f_0 < 3700$	18

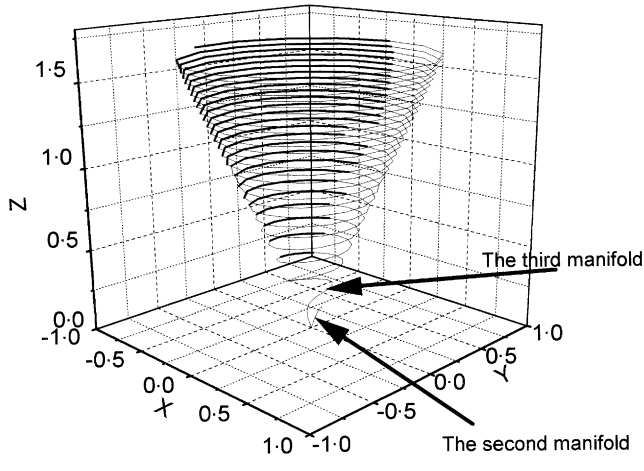

Figure 5. The invariant manifolds.

$a_2 = 0$ at $\mu = 0{\cdot}05$, $\sigma = 0.6$, $f_0 = 100$. The second manifold with tangent vector U_2 is unstable. Therefore to obtain this manifold the integration in forward time was carried out. This manifold corresponds to motion (CA) in region (GLC_1F) (see Figure 3(b)). The third manifold is stable. It has the tangent vector U_3. To obtain this manifold, the integration in reverse time was carried out. As the result of the calculations we come to the conclusion that the invariant manifolds behavior is topologically equivalent to the pattern shown in Figure 3(b).

6. BEAM OSCILLATIONS QUALITATIVE PROPERTIES

The two previous sections were devoted to the modulation equations. Now these results are used to analyze qualitative properties of beam oscillations. The steady oscillations are

$$w = \sqrt{2}a_1 \cos(v_1 t - C_*) \sin(\pi x) + \frac{a_1}{\sqrt{2}} \cos(v_2 t + C_* - \gamma^0) \sin(2\pi x) + \psi(x,t) + O(\varepsilon), \tag{53}$$

where $\gamma^0 = \arcsin(\mu\pi^6/2f_0^2\chi_1)$ is the variable of the fixed point of equation (8). Frequencies v_1 and v_2 have the form:

$$v_j = j^2\pi^2 + \varepsilon\Omega_j + O(\varepsilon^2),$$
$$\Omega_j = \frac{3}{16}\pi^2 a_1^2 + \frac{6f_0^2}{\pi^6}\rho_j + \frac{\pi^2}{2}a_2^2 + 2F\cos(\gamma), \quad j = 1,2, \tag{54}$$

where $\rho_1 + \rho_2 = \chi$, $\rho_1 = 4{\cdot}73 \cdot 10^{-3}$, $\rho_2 = 5{\cdot}09 \times 10^{-3}$. Using equations (8), we obtain the relation

$$v_1 + v_2 = 2\Omega + O(\varepsilon^2). \tag{55}$$

Note that oscillations (53) have two frequencies v_1 and v_2 and their combination Ω. The oscillations are almost-periodic, if $nv_1 + mv_2 \neq 0$, where m, n are positive integer numbers. It is known, that if frequencies v_1 and v_2 are changed a little, almost-periodic oscillations may be transformed into periodic. Let us prove the theorem.

Theorem 7. *Beam oscillations* (53) *are always almost-periodic.*

Proof. On the assumption that oscillations (53) are periodic:

$$v_1 = \frac{m}{n}v_2. \tag{56}$$

If equations (54) are substituted into equation (56), two relations are obtained:

$$\frac{m}{n} = \frac{1}{4}, \qquad \frac{5}{16}\pi^2 a_1^2 - \frac{p}{2} + \frac{8f_0^2\rho_1}{\pi^6} = \frac{2f_0^2\rho_2}{\pi^6}. \tag{57}$$

Now the proof is developed separately for sheets A and B (see Figure 3(a)). Let us consider sheet A. If formula (28) is substituted into equation (57), the following equation is obtained:

$$\sigma = 10\frac{f_0^2}{\pi^6}(\rho_2 - \rho_1). \tag{58}$$

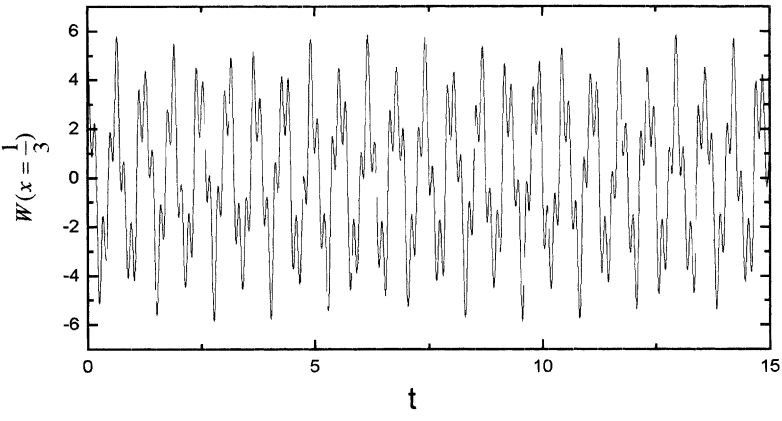

Figure 6. The stable almost-periodic beam oscillations.

The curve (58) does not intersect the sheet A. Therefore, the oscillations are almost-periodic. Let us consider sheet B. The periodic oscillations curve has the form:

$$\sigma = 2\sqrt{16\frac{f_0^4\chi_1^2}{\pi^{12}} - 4\mu^2} + 10\frac{f_0^2}{\pi^6}(\rho_2 - \rho_1). \tag{59}$$

This curve does not pass through sheet B. Therefore, the oscillations are almost-periodic.

The qualitative properties of the fixed points and the beam oscillations connect in the following way.

(1) Stable (unstable) trivial solution $x = y = z = 0$ of equations (10) corresponds to the beam stable (unstable) periodic oscillations with period $T = 2\pi/\Omega$.
(2) The stable (unstable) nontrivial fixed points of equations (10) correspond to the stable (unstable) almost-periodic oscillations of a beam.
(3) The pitchfork bifurcations correspond to the appearance of the beam almost-periodic oscillations. These oscillations arise from the periodic vibrations.
(4) The system's (10) saddle-node bifurcation corresponds to the junction of two almost-periodic motions.

The stable almost-periodic oscillations of beam point $x = \frac{1}{3}$ at $(\sigma, f_0) = (65; 512{\cdot}8)$ are shown in Figure 6. The beam deflections at instants $\pi/5\Omega; 2\pi/5\Omega; 3\pi/5\Omega;\ 4\pi/5\Omega; \pi/\Omega;$ $6\pi/5\Omega$ are shown in Figure 7.

7. NUMERICAL SIMULATIONS OF BEAM OSCILLATIONS

It is known that results of the perturbation methods differ from data of numerical simulations [47, 48]. For example, numerical integration of the weak non-linear oscillator with periodic force exhibits chaos. On the other hand, chaos can not be predicted by the perturbation techniques in this system. It is known, that solutions of the perturbation methods are correct at $0 < \varepsilon < \varepsilon_*\ (\varepsilon_* \ll 1)$ [48]. The value of ε_* is not known previously. We stress that if the system parameters approach to bifurcation points, the value of ε_* is decreased quickly. Therefore, in this paper the analytical results are supplemented by numerical simulations.

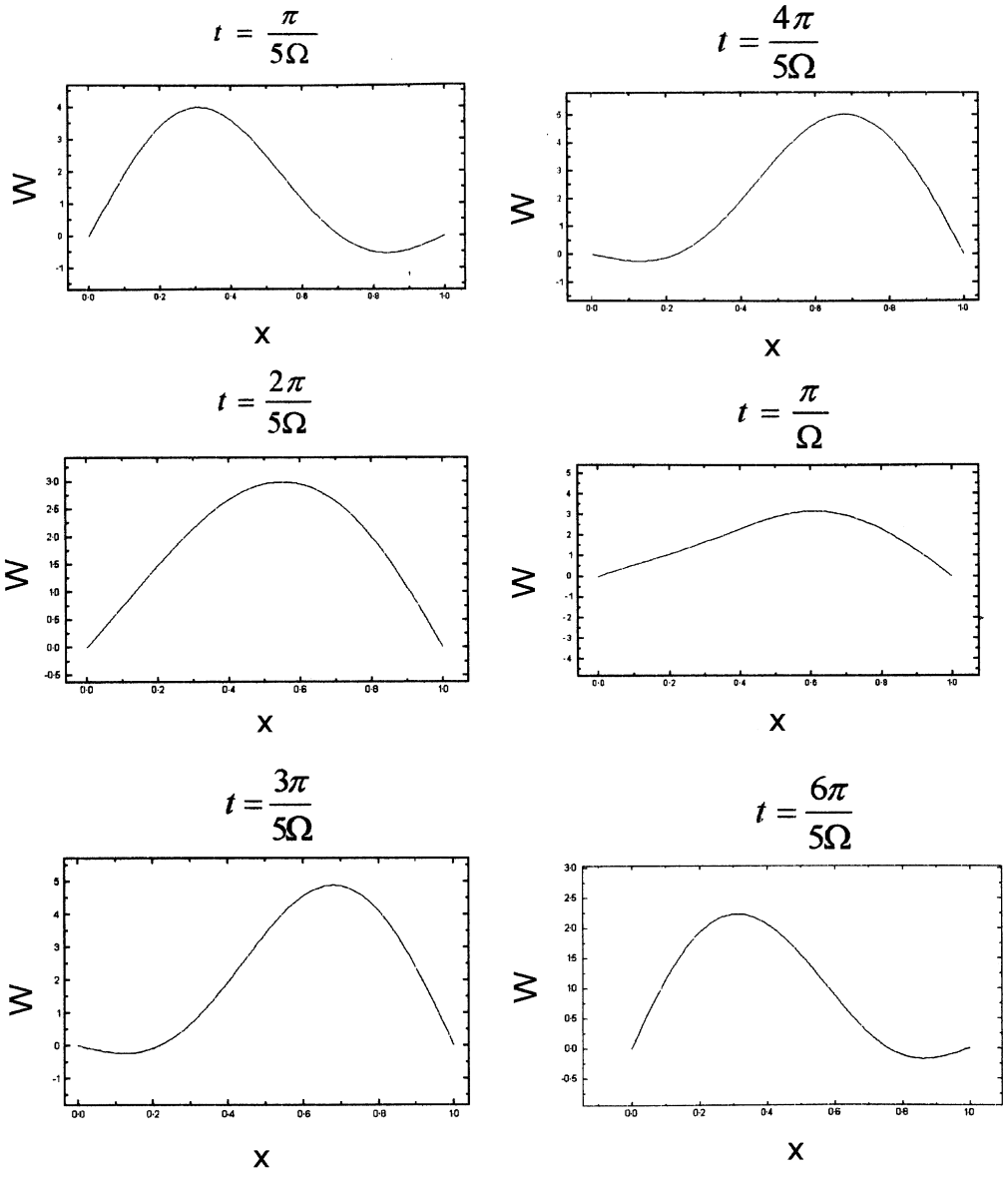

Figure 7. The beam deflections at instants $\pi/5\Omega; 2\pi/5\Omega; 3\pi/5\Omega; 4\pi/5\Omega; \pi/\Omega; 6\pi/5\Omega$.

System (4) is reduced to two differential equations. Using equation (4), we obtain $\eta_{3n} = 0; n = 1, 2, \ldots$ Assuming $\eta_1 \neq 0; \eta_2 \neq 0;$ and $\eta_{3n-2} = \eta_{3n-1} = 0; n = 2, 3 \ldots$, system (4) has the form:

$$\begin{aligned} \ddot{\eta}_1 + \pi^4 \eta_1 &= \varepsilon\left(-\frac{\pi^4}{2}\eta_1(\eta_1^2 + 4\eta_2^2) - 2\mu\dot{\eta}_1\right) + \sqrt{1{\cdot}5} f_0 \cos(\Omega t), \\ \ddot{\eta}_2 + 16\pi^4 \eta_2 &= \varepsilon(-2\pi^4 \eta_2(\eta_1^2 + 4\eta_2^2) - 2\mu\dot{\eta}_2) + \sqrt{1{\cdot}5} f_0 \cos(\Omega t). \end{aligned} \tag{60}$$

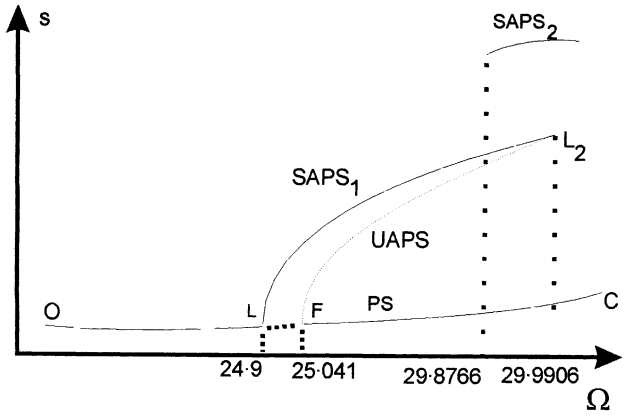

Figure 8. The bifurcation diagram, where force frequency Ω is shown against the oscillations swing.

Note that system (60) has the symmetric solutions:

$$\eta_1(t) = -\eta_1\left(t + \frac{T}{2}\right), \quad \eta_2(t) = -\eta_2\left(t + \frac{T}{2}\right). \tag{61}$$

The aim of the calculations is to analyze bifurcations of dynamical system (60). The bifurcation behavior is presented qualitative on the bifurcation diagram (Figure 8), which shows frequency Ω versus the swing of oscillations. The stable and unstable states are denoted by the solid and dotted curves respectively. To obtain this diagram, system (60) was integrated numerically using the fourth order Runge–Kutta method with a constant step size. Motions were considered transient at $0 < t < 6 \times 10^4\pi/\Omega$. The steady motions were analyzed at $6 \times 10^4\pi/\Omega < t < 9 \times 10^4\pi/\Omega$ by means of the Poincare map. To obtain the Poincare map, variables $\eta_1(t), \dot{\eta}_1(t)$ at $t_j = j2\pi/\Omega$, $30\,000 < j < 45\,000$ were plotted on the plane. We take the following parameters $f_0 = 1000$, $\mu = 0{\cdot}5$, $\varepsilon = 1 \times 10^{-2}$. We stress that this bifurcation diagram is similar to the frequency response obtained by the perturbation methods. Diagram section (OL) shows the periodic oscillations. The Naimark–Sacker bifurcation takes place in point $L(\Omega_L = 24{\cdot}9)$. In this case the stable periodic motions are transformed into the unstable oscillations and the stable almost-periodic orbits arise. Note that the value of Ω_L is equal to the value obtained by the perturbation methods. Diagram part (LL_2) shows the almost-periodic oscillations. As an example, Figure 9(a) shows the Poincare sections of the almost-periodic oscillations at $\Omega = 29{\cdot}6$ and Figure 10(a) shows $\eta_1(t)$. We stress that stable almost-periodic solutions $SAPS_1$ and unstable almost-periodic solutions $UAPS$ are merged. Now the almost-periodic motions close to point L_2 is considered when Ω is increased. In this case, the dynamical system approaches to point L_2 on branch $SAPS_1$. In L_2 the oscillations breakdown are observed, i.e. if Ω is increased, the motions are attracted to branch $SAPS_2$. Figure 9(b) shows the Poincare sections of these oscillations at $\Omega = 29{\cdot}95$ and Figure 10(b) shows $\eta_1(t)$. Section (CF) (Figure 8) describes the periodic oscillations. The Naimark–Sacker bifurcation takes place at point $F(\Omega_F = 25{\cdot}04)$. If Ω is decreased, the stable periodic oscillations are transformed into the unstable motions and the unstable almost-periodic oscillations are arisen. Point $F(\Omega_F = 25{\cdot}06)$ is predicted by the perturbation methods.

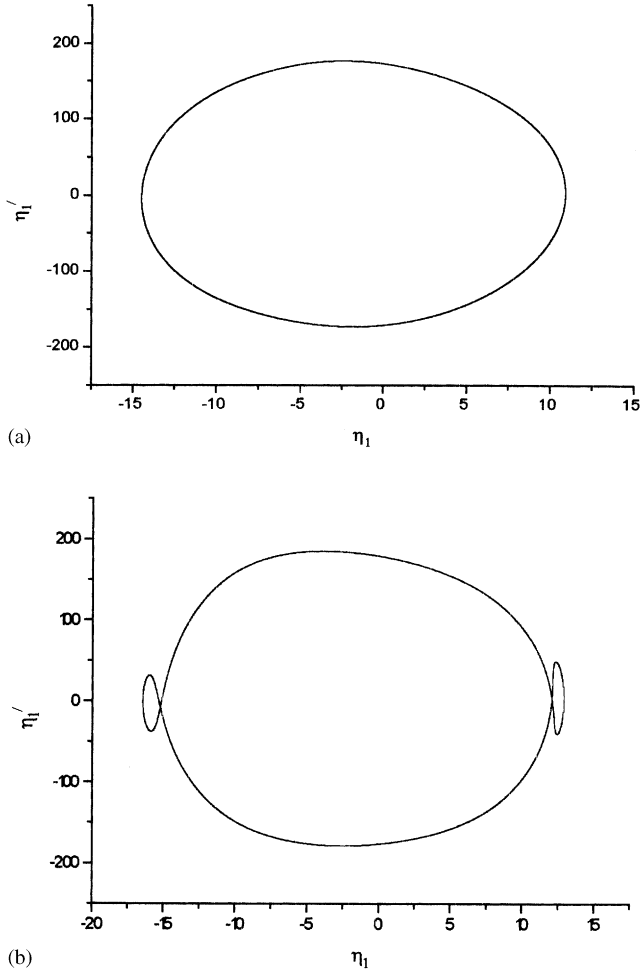

Figure 9. The Poincare sections of the almost-periodic oscillations: (a) $\Omega = 29{\cdot}6$; (b)-$\Omega = 29{\cdot}95$.

8. CONCLUSION

The beam plane oscillations at the combination resonance are considered in this paper. The non-linear membrane stiffness is taken into account in the beam model. To analyze the combination resonance, the many-mode approximation of oscillations is considered. Using the Galerkin method, the system of the ordinary differential equations is obtained. Three autonomous differential equations are derived by the multiple scales method. This dynamical system's qualitative properties are expressed in six theorems. The steady states of this system are analyzed numerically. It is shown analytically, that two Naimark–Sacker bifurcations at the combination resonance are observed. These bifurcations are analyzed by the center manifold method.

ACKNOWLEDGMENTS

The author expresses thanks to Professor O. Morachkovsky (Department of Theoretical Mechanics, National Technical University "Kharkov Polytechnical Institute") and to

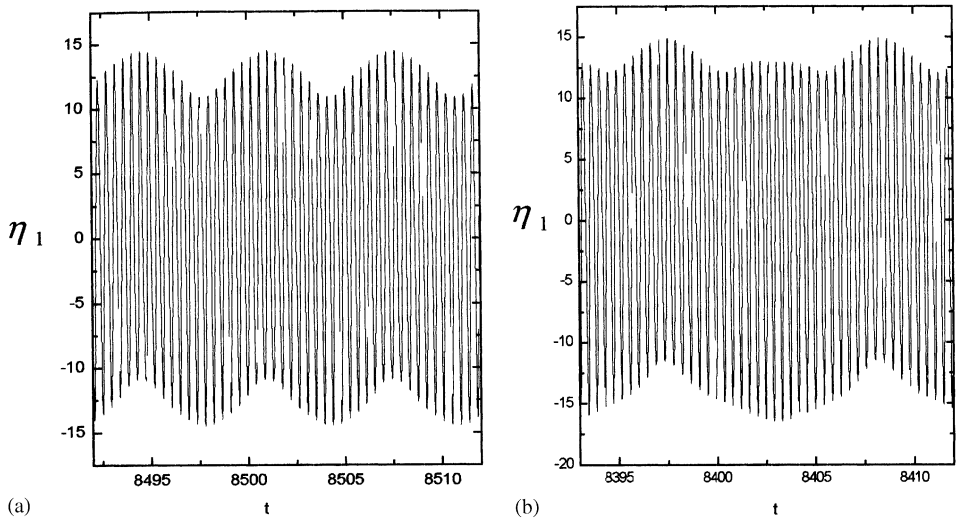

Figure 10. The almost-periodic oscillations: (a) $\Omega = 29{\cdot}6$; (b) $\Omega = 29{\cdot}95$.

Professor Yu. Mikhlin (Department of Applied Mathematics, National Technical University "Kharkov Polytechnical Institute") for the helpful discussions.

REFERENCES

1. S. Woinowsky-Krieger 1950 *American Society of Mechanical Engineers Journal of Applied Mechanics* **17**, 35–36. The effect of an axial force on the vibration of hinged bars.
2. R. S. Langley 1987 *Journal of Sound and Vibration* **116**, 390–393. The effect of linearization and longitudinal deformation on the predicted response of non-linear beams.
3. H. Wagner 1965 *American Society of Mechanical Engineers Journal of Applied Mechanics* **32**, 887–892. Large-amplitude free vibrations of a beam.
4. P. H. McDonald and N. C. Raleigh 1955 *American Society of Mechanical Engineers Journal of Applied Mechanics* **22**, 573–578, Nonlinear dynamic coupling in a beam vibration.
5. D. A. Evensen 1967 *American Institute of Aeronautics and Astronautics Journal* **6**, 370–372. Nonlinear vibrations of beams with various boundary conditions.
6. A. H. Nayfeh 1973 *Journal of the Acoustical Society of America* **53**. Nonlinear transverse vibrations of beams with properties that vary along the length.
7. W. J. Tseng and J. Dugundji 1970 *American Society of Mechanical Engineers Journal of Applied Mechanics* **37**, 292–297. Nonlinear vibrations of a beam under harmonic excitation.
8. W. Y. Tseng and J. Dugundji 1971 *American Society of Mechanical Engineers Journal of Applied Mechanics* **38**, 467–472. Nonlinear vibrations of a buckled beam under harmonic excitation.
9. A. Luongo and G. Rega and F. Vestroni 1986 *American Society of Mechanical Engineers Journal of Applied Mechanics* **53**, 619–624. On nonlinear dynamics of planar shear indeformable beams.
10. C. L. Lou and D. L. Sikarskie 1975 *American Society of Mechanical Engineers Journal of Applied Mechanics* **209**, 209–214. Nonlinear vibration of beams using a form-function approximation.
11. R. F. Fung 1997 *Journal of Sound and Vibration* **203**, 373–387. The affect of nonlinear inertia on the steady state response of a beam system subjected to combination excitations.
12. Y. Dong and G. Xie and J. Y. K. Lou 1992 *Ocean Engineering* **19**, 555–571. Stability of vortex-induced oscillations of tension leg platform tethers.

13. J. A. Bennet and J. G. Eisley 1970 *American Institute of Aeronautics and Astronautics Journal* **1**, 734–739. A multiple degree-of-freedom approach to nonlinear beam vibrations.
14. J. A. Bennet 1973 *American Institute of Aeronautics and Astronautics Journal* **11**, 710–715. Ultraharmonic motion of viscously damped nonlinear beam.
15. A. H. Nayfeh and D. T. Mook and S. Sridhar 1974 *Journal of the Acoustical Society America* **55**, 281–291. Nonlinear analysis of the forced response of structural elements.
16. D. M. Tang and E. H. Dowell 1988 *American Society of Mechanical Engineers Journal of Applied Mechanics* **55**, 190–196. On the threshold force for chaotic motions for a forced buckled beam.
17. A. H. Nayfeh and D. T. Mook 1979 *Nonlinear oscillations*. New York: John Wiley and Sons.
18. H. A. Evensen and R. M. Evan-Iwanowski 1966 *American Society of Mechanical Engineers Journal of Applied Mechanics* **33**, 144–148. Effects of longitudinal inertia upon the parametric response of elastic column.
19. K. Eisinger and H. C. Merchant 1979 *American Society of Mechanical Engineers Journal of Applied Mechanics* **46**, 197–202. Clamped beam parametric amplifier.
20. K. Sato, H. Saito and K. Otomi 1978 *American Society of Mechanical Engineers Journal of Applied Mechanics* **45**, 643–648. The parametric response of a horizontal beam carring a concentrated mass under gravity.
21. V. Kovalov and M. Rozovski 1985 *Applied Mechanics* **21**, 126–129. The main parametric responce of the viscoelasticity beam transverse oscillations in the nonlinear formulation (in Russian).
22. Hoang-Van-Da 1985 *Applied Mechanics* **21**, 85–88. Beam parametric oscillations with regard to nonlinear elastic heredity of material.
23. V. V. Bolotin 1964 *The Dynamic Stability of Elastic Systems*. Holden-Day: San Francisco.
24. M. R. M. Crespo da Silva and C. C. Glynn 1979 *International Journal of Solids and Structures* **15**, 209–219. Non-linear non-planar resonant oscillations in fixed–free beams with support asymmetry.
25. M. R. M. Crespo da Silva 1980 *American Society of Mechanical Engineers Journal of Applied Mechanics* **47**, 409–414. Nonlinear response in a column subjected to a constant end force.
26. A. Luongo, G. Rega and F. Vestroni 1989 *Journal of Sound and Vibration* **134**, 73–86. Non-resonant non-planar free motions of inextensional non-compact beams.
27. E. C. Haight and W. W. King 1972 *Journal of the Acoustical Society of America* **52**, 899–911. Stability of nonlinear oscillations of an elastic rod.
28. P. F. Pai and A. H. Nayfeh 1990 *International Journal of Non-linear Mechanics* **25**, 455–474. Non-linear non-planar oscillations of a cantilever beam under lateral base excitations.
29. I.-M. K. Shyu and D. T. Mook, R. H. Plaut. 1993 *Nonlinear Dynamics* **4**, 227–249. Whirling of a forced cantilevered beam with static deflection I: Primary resonance.
30. I.-M. K. Shyu, R. H. Plaut and D. T. Mook. 1993 *Nonlinear Dynamics* **4**, 337–356. Whirling of a forced cantilevered beam with static deflection II: Superharmonic and Subharmonic Resonances.
31. F. C. Moon 1987. *Chaotic Vibrations*. New York: John Wiley and Sons.
32. A. H. Nayfeh 1981. *Introduction to Perturbation Techniques*. New York: John Wiley and Sons.
33. J. A. Sanders and F. Verhulst 1985. *Averaging Methods in Nonlinear Dynamical Systems*. Berlin: Springer-Verlag.
34. E. N. Lorenz 1963 *Journal of the Atmospheric Sciences* **20**, 130–141. Deterministic nonperiodic flow.
35. J. Marsden 1977 *Lecture Notes in Mathematics* 615. Attempts to relate the Navier–Stokes equations to turbulence.
36. P. Gaspard and G. Nicolis 1983 *Journal of Statistical Physics* **31**, 437–445. What can we learn from homoclinic orbits in chaotic dynamics?
37. R. Lozi and S. Ushiki 1991 *International Journal of Bifurcation and Chaos* **1**, 923–926, Coexisting chaotic attractors in Chua's circuit.
38. A. K. Bajaj and S. Tousi 1990 *International Journal of Non-Linear Mechanics* **25**, 625–641. Torus doublings and chaotic amplitude modulations in a two degree-of-freedom resonantly forced mechanical system.
39. A. H. Nayfeh, B. Balachandran 1991 *Nonlinear Phenomena Conference, Moscow, USSR*. Nonlinear response of resonantly forced dynamical and structural systems.
40. O. M. O'Reilly 1993 *International Journal of Non-Linear Mechanics* **28**, 337–351. Global bifurcations in the forced vibration of a damped string.

41. Y. A. KUZNETSOV 1995 *Elements of Applied Bifurcation Theory*. Berlin: Springer-Verlag.
42. S. WIGGINS 1990 *Introduction to Applied Nonlinear Dynamical Systems and Chaos*. Berlin: Springer-Verlag.
43. P. J. HOLMES and D. A. RAND 1976 *Journal of Sound and Vibration* **44**, 237–253. The bifurcations of Duffing's equation:an application to catastrophe theory.
44. J. GUCKENHEIMER and P. J. HOLMES 1983 *Nonlinear Oscillations, Dynamical Systems and Bifurcations of Vector Fields*. New York, Heidelberg, Berlin: Springer-Verlag.
45. T. S. PARKER and L. O. CHUA 1989 Practical numerical algorithms for chaotic systems. New York: Springer-Verlag.
46. J. SHAW, S. W. SHAW and A. G. HADDOW 1989 *International Journal of Non-Linear Mechanics* **24**, 281–293.On the response of the nonlinear vibration absorber.
47. N. HAQUANG, D. T. MOOK and R. H. PLAUT 1987 *Journal of Sound and Vibration* **118**, 425–439. A non-linear analysis of the interaction between parametric and external excitations.
48. J. M. JOHNSON and A. K. BAJAJ 1989 *Journal of Sound and Vibration* **128**, 87–107. Amplitude modulated and chaotic dynamics in resonant motion of strings.

APPENDIX A

$$r_1 = \frac{\delta[\chi_1 v(w-v) - \mu v]}{2(2\chi_1 v + \mu)} + \frac{5\pi^2}{16}(v-w)(v^2+w^2+2u^2),$$

$$r_2 = -\frac{\delta^2(v+w)}{8(2\chi_1 v+\mu)} - \frac{5\pi^2}{8}u(v^2+w^2+2u^2),$$

$$f_1 = \frac{5\pi^2\sqrt{\delta_1}}{8}\left[z_1^2 + 4x_1^2 + 12y_1^2 + 4z_1y_1 + \frac{y_1}{2\sqrt{\delta_1}}(z_1^2+4x_1^2+4y_1^2)\right]$$

$$+ \frac{x_1}{z_1+4\sqrt{\delta_1}}[\mu z_1 - 2(\mu+2\chi_1 v)y_1 - 8\chi_1 v\sqrt{\delta_1}],$$

$$f_2 = \chi_1 v(z_1+4\sqrt{\delta_1}) - \frac{5\pi^2}{16}x_1[8\sqrt{\delta_1}(z_1+2y_1) + z_1^2 + 4x_1^2 + 4y_1^2] + \frac{2(\mu+2\chi_1 v)x_1^2}{z_1+4\sqrt{\delta_1}},$$

$$f_3 = 4\chi_1 v(y_1 + 2\sqrt{\delta_1}),$$

$$F_1 = -2\chi_1 v\left(v + \frac{2\delta\sqrt{\delta_1}}{\mu}\right) + \frac{5\pi^2}{4}\sqrt{\delta_1}\left[2u^2 + \left(2 + 12\frac{\mu^2}{\delta^2}\right)v^2 + w^2 + 4v\left(u + \frac{\mu}{\delta}w\right)\right]$$

$$+ \frac{5\pi^2}{8}\left(\frac{\mu}{\delta}v - \frac{w}{2}\right)\left[\frac{4\mu^2}{\delta^2}v^2 + w^2 + 2(u+v)^2\right]$$

$$+ \left(\frac{2\mu}{\delta}v + w + 4\sqrt{\delta_1}\right)^{-1}[(u+v)(2\mu w - 8\sqrt{\delta_1}\chi_1 v) - \delta(u+v)^2],$$

$$F_2 = \frac{\delta}{\mu}\left[2\chi_1 v\left(2\sqrt{\delta_1} + \frac{\mu}{\delta}v\right) - \frac{1}{2}\rho(u,v,w)\right],$$

$$F_3 = -2\chi_1 vw + \rho(u, v, w),$$

$$\rho(u, v, w) = \frac{\mu}{\sqrt{\delta_1}} v(u+v) + \frac{5\pi^2}{8}\left[2(u+v)^3 + (u+v)\left(\frac{4\mu^2}{\delta^2} v^2 + w^2\right)\right]$$

$$- 2\mu(u+v)^2\left[\frac{2\mu}{\delta} v + w + 4\sqrt{\delta_1}\right]^{-1}.$$